Geometric Accuracy of 3-D X-Ray Image-Based Localization from Two C-Arm Views

Alexander Brost[1], Norbert Strobel[2], Liron Yatziv[3], Wesley Gilson[4], Bernhard C. Meyer[5], Joachim Hornegger[1], Jonathan S. Lewin[6], and Frank K. Wacker[6]

[1] Chair of Pattern Recognition, Department of Computer Science,
Friedrich-Alexander-University, Erlangen-Nuremberg, Erlangen, Germany
`Alexander.Brost@informatik.uni-erlangen.de`
[2] Siemens AG, Healthcare Sector, Forchheim, Germany
[3] Siemens Corporate Research, Imaging and Visualization, Princeton, NJ, USA
[4] Siemens Corporate Research, Imaging and Visualization, Baltimore, MD, USA
[5] Klinik und Hochschulambulanz für Radiologie und Nuklearmedizin, Charité
Universitätsmedizin Berlin, Campus Benjamin Franklin, Berlin, Germany
[6] The Russell H. Morgan Department of Radiology and Radiological Science, The
Johns Hopkins University School of Medicine, Baltimore, MD, USA

Abstract. Image guided interventions often involve C-arm X-ray imaging systems. State-of-the art fluoroscopy systems not only offer 2-D X-ray imaging, but they can also be used to obtain 3-D cone-beam tomographic data sets. These 3-D volumetric images can be used for image guidance and device navigation. To navigate a device with confidence, it is, however, important to know where it is with respect to the volume. We addressed this question by evaluating the geometric accuracy of 3-D X-ray image-based localization from two C-arm views. To this end a simulation study was performed first. The results of this study are compared with a phantom experiment involving a real C-arm system. The phantom design comprised five point-like objects arranged in such a way that they could be distinguished in all possible viewing directions. The same point configuration was used for simulation study and experiment. For the simulation study, these five 3-D points were forward projected assuming an ideal C-arm imaging geometry. The resulting point coordinates at the detector were then disturbed by Gaussian noise (standard deviation: 1.232 mm). Finally, 3D point localization was performed by triangulation from two views again assuming an ideal C-arm system geometry. The error for two imaging views was calculated as the Euclidean distance between the localized and the original 3-D points and averaged over the five objects. For the (real) experiment, the idealized projection matrices were replaced by actual projection matrices returned by the system. The simulation results yielded a minimal localization error of 0.81 mm. In the experiment, a minimal error of 0.99 mm was achieved.

1 Introduction

C-arm devices are X-ray systems that have their detector and X-ray source mounted to a C-shaped gantry. Among others, these systems are used for mini-

mally"=invasive, local therapy under fluoroscopic guidance. C-arm devices also offer the possibility to acquire 3-D data sets using C-arm computed tomography techniques (C-arm CT), e.g., using *syngo* DynaCT (Siemens AG, Healthcare Sector, Forchheim, Germany) [1, 2]. To perform C-arm CT, the knowledge of the projection geometry is essential. It is obtained by calibration, e.g., as described in [3]. The resulting projection matrices can also be used to render 2-D images from 3-D data sets. These so-called overlay images can be combined with live fluoroscopic scenes for image-guided interventions [4]. Stereotactic approaches for punctures [5, 6] and breast biopsy [7] are used in clinical applications as well. In this case, the 3-D position of a target point is obtained by identifying the instrument from two different viewing angles and computing its 3-D coordinates by triangulation. System accuracy is important for such procedures, as misguided punctures may put the patient at higher risk. To study the localization error, we present a mathematical model for the projection geometry of a C-arm system. Then we evaluate how a 2-D error at the detector affects 3-D point localization using a simulation based on an idealized C-arm geometry. We also show the results of an experiment involving a real Artis dFA C-arm system (Siemens AG, Healtcare Sector, Forchheim, Germany).

2 Methods

Point reconstruction in 3-D from two views requires knowledge of the projection geometry for each of the projection images [8]. Modern C-arm systems are calibrated [3], such that their projection matrices are known. C-arm calibration tries to compensate for the non-ideal system geometry [9]. In the following, a mathematical model to compute the projection matrices of a C-arm system is introduced.

2.1 Idealized Projection Geometry of a C-Arm

For high-end C-arm systems, it is possible to use the pinhole camera model to describe the projection geometry of a C-arm system [8]. This involves a projection matrix $\mathbf{P} \in \mathbb{R}^{3\times 4}$ defined as [8]

$$\mathbf{P} = \mathbf{K}[\mathbf{R}|\mathbf{t}] \tag{1}$$

with $\mathbf{K} \in \mathbb{R}^{4\times 3}$ representing the intrinsic camera parameters. The matrix $\mathbf{R} \in \mathbb{R}^{3\times 3}$ and the vector $\mathbf{t} \in \mathbb{R}^3$ comprise the extrinsic camera parameters for rotation and translation, respectively. The intrinsic camera parameters depend on the the source-to-image-distance (SID), the pixel spacing of the detector p and the image coordinates of the projected iso-center at the imaging plane o_u and o_v. As the X-ray images are usually rotated by 90° before shown on a monitor, this (fixed) rotation is often added to the intrinsic camera parameters, thus resulting in

$$\mathbf{K} = \begin{pmatrix} \frac{\text{SID}}{p} & 0 & o_x \\ 0 & \frac{\text{SID}}{p} & o_y \\ 0 & 0 & 1 \end{pmatrix} \cdot \begin{pmatrix} 1 & 0 & 0 \\ 0 & 0 & -1 \\ 0 & 1 & 0 \end{pmatrix}. \tag{2}$$

Considering the geometry of a C-arm system as shown in Fig. 1, we see that the extrinsic parameters depend on the source-to-isocenter-distance (SISOD) as the translational part and the rotation angles α and β, also considered as primary and secondary angle, respectively. The translation depends on the mechanical design of the C-arm and is given by the distance of the X-ray source to the iso-center, the origin of the coordinate system for a C-arm. The primary angle (RAO/LAO) denotes the rotation of a C-arm related to a patient's right/left side (right anterior oblique/left anterior oblique). The secondary angle (CRAN/CAUD) denotes the rotation towards a patient's head (cranial) or feet (caudal) direction. If the system has been properly positioned, the translation can be denoted as

$$\mathbf{t} = (0 \;\; \text{SISOD} \;\; 0)^T. \tag{3}$$

The rotation matrix $\mathbf{R}_\alpha$ for the primary angle is given as

$$\mathbf{R}_\alpha = \begin{pmatrix} \cos(\alpha) & \sin(\alpha) & 0 \\ -\sin(\alpha) & \cos(\alpha) & 0 \\ 0 & 0 & 1 \end{pmatrix} \tag{4}$$

with the angle α in RAO/LAO view direction. The rotation matrix for the secondary angle is given as

$$\mathbf{R}_\beta = \begin{pmatrix} 1 & 0 & 0 \\ 0 & \cos(\beta) & \sin(\beta) \\ 0 & -\sin(\beta) & \cos(\beta) \end{pmatrix} \tag{5}$$

with the angle β in CRAN/CAUD view direction. It is important to note that the angles, α and β, are anatomical angles related to patient position. To calculate the projection matrices, we use the anatomical angles that are used to define the exact position of the detector on the sphere the C-arm is moving on. In fact, there are two sphere, one with a radius of the isocenter-to-image-distance ISOID on which the detector is moving on, and one with a radius of SISOD for the X-ray source. The distance of the detector to the X-ray source is called source-to-image-distance SID and given by

$$\text{SID} = \text{SISOD} + \text{ISOID}. \tag{6}$$

The overall camera rotation can be calculated as

$$\mathbf{R} = \mathbf{R}_\alpha \cdot \mathbf{R}_\beta. \tag{7}$$

2.2   Point Localization from Two Views

An algorithm for point reconstruction from two views was presented in [8], considering only one (primary) angle. This algorithm is extended below to consider the secondary angle as well. Using the projection matrix given in Eq. (1), the projection of a point $\mathbf{w}$ in 3-D space is calculated as

$$\tilde{\mathbf{v}}_{\alpha,\beta} = \mathbf{P} \cdot \tilde{\mathbf{w}} \tag{8}$$
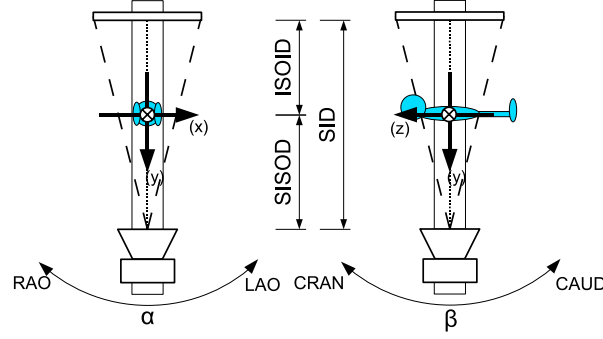
Fig. 1. Basic projection view geometry of a C-arm X-ray imaging system: SID denotes the source-to-image-distance, SISOD the source-to-isocenter-distance and ISOID the isocenter-to-image distance. The iso-center is at the origin of the world coordinate system.

with $\tilde{\mathbf{v}}_{\alpha,\beta} \in \mathbb{R}^3$ representing the resulting 2-D point in the imaging plane in homogeneous coordinates and $\tilde{\mathbf{w}} = (\mathbf{w}^T\ 1)^T$ representing the world point also in homogeneous coordinates. As the fourth component of the vector $\tilde{\mathbf{w}}$ is 1, the projection can be rewritten as

$$\tilde{\mathbf{v}}_{\alpha,\beta} = \mathbf{K}\left(\mathbf{R} \cdot \mathbf{w} + \mathbf{t}\right) \tag{9}$$

by using Eq. (1). This equation can be solved for the world point $\mathbf{w}$ in non-homogeneous coordinates and we get

$$\mathbf{w} = \mathbf{R}^{-1} \cdot \left(\mathbf{K}^{-1} \cdot \tilde{\mathbf{v}}_{\alpha,\beta} - \mathbf{t}\right). \tag{10}$$

Since the 2-D point $\tilde{\mathbf{v}}_{\alpha,\beta}$ in the imaging plane is given in homogeneous coordinates, its exact coordinates are only known up to a scaling factor $\tau \in \mathbb{R}$. Therefore, we can write

$$\tilde{\mathbf{v}}_{\alpha,\beta} = \begin{pmatrix} \tau u_{\alpha,\beta} \\ \tau v_{\alpha,\beta} \\ \tau \end{pmatrix} = \begin{pmatrix} \tau \mathbf{v}_{\alpha,\beta} \\ \tau \end{pmatrix} = \tau \begin{pmatrix} \mathbf{v}_{\alpha,\beta} \\ 1 \end{pmatrix} = \tau \mathbf{v}_{\alpha,\beta}^{\star} \tag{11}$$

with $\mathbf{v}_{\alpha,\beta}^{\star} = (\mathbf{v}_{\alpha,\beta}, 1)^T$ and $\mathbf{v}_{\alpha,\beta} = (u_{\alpha,\beta}, v_{\alpha,\beta})^T$ representing the actual 2-D coordinates in the imaging plane for the viewing angles α and β. Replacing $\tilde{\mathbf{v}}_{\alpha,\beta}$ by $\tau \mathbf{v}_{\alpha,\beta}^{\star}$, we get a line equation connecting the optical center and the point $\mathbf{v}_{\alpha,\beta}$ in the imaging plane in 3-D space. A point on this line is given by

$$\begin{aligned} \mathbf{r}_{\alpha,\beta}(\tau) &= \mathbf{R}^{-1} \cdot \left(\mathbf{K}^{-1} \cdot \tau \cdot \mathbf{v}_{\alpha,\beta}^{\star} - \mathbf{t}\right) \\ &= \tau \cdot \mathbf{R}^{-1}\mathbf{K}^{-1}\mathbf{v}_{\alpha,\beta}^{\star} - \mathbf{R}^{-1} \cdot \mathbf{t} \tag{12} \\ &= \mathbf{o}_{\alpha,\beta} + \tau \cdot \mathbf{d}_{\alpha,\beta} \tag{13} \end{aligned}$$

with the optical center $\mathbf{o}_{\alpha,\beta} = -\mathbf{R}^{-1} \cdot \mathbf{t}$ as the point of origin and the direction vector $\mathbf{d}_{\alpha,\beta} = \mathbf{R}^{-1}\mathbf{K}^{-1}\mathbf{v}_{\alpha,\beta}^{\star}$. As shown in [8], two views are required to localize a point in 3-D space. The first view is given by the viewing angles α_1 and β_1 and the second view is given by α_2 and β_2. Using Eq. (13), two rays in 3-D space can be calculated by

$$\mathbf{w} = \mathbf{o}_{\alpha_1,\beta_1} + \nu\mathbf{d}_{\alpha_1,\beta_1} \tag{14}$$

$$\mathbf{w} = \mathbf{o}_{\alpha_2,\beta_2} + \mu\mathbf{d}_{\alpha_2,\beta_2} \tag{15}$$

with $\nu, \mu \in \mathbb{R}$. Due to errors during the selection of points in 2D projections associated with the same 3D object, the lines need not necessarily intersect. This is why we take the closest point between those two rays as a solution calculated using a least squares approach.

2.3   Localization Error

The 3-D localization error is computed as the Euclidean distance between the localized point from two views and the original 3-D point. To this end, we forward project the original 3-D point and disturbed the resulting 2D positions by adding Gaussian noise with a standard deviation of 1.232 mm in each of eight 2-D direction. As the phantom contained five points, the 3-D localization error for two angulations, (α_1, β_1) and (α_2, β_2), is the average over the localization error of all five points. Using this approach, the influence of outliers is reduced. For analysis and comparison, the localization error dependent on two angulations, given by (α_1, β_1) and (α_2, β_2), is averaged over all viewing angles that have identical angular differences. The primary angular difference is given by $\Delta\alpha = |\alpha_1 - \alpha_2|$ and the secondary angular difference by $\Delta\beta = |\beta_1 - \beta_2|$. We use relative angles, because they are more relevant for 3-D localization.

3   Simulation and Experiment

The phantom used as ground truth for our simulation and experiments comprised five point-like objects, arranged such that their shadows showed minimal overlap when acquiring X-ray projections from various viewing angles. The physical phantom was a box filled with gelatin of size 15 cm x 10 cm x 5 cm with radio-opaque sphere-shaped objects with a diameter of 2 mm. The system used to for the experiment was a clinical floor-mounted C-arm device (AXIOM Artis dFA, Siemens AG, Healthcare Sector, Forchheim, Germany) at the Johns Hopkins Hospital (Baltimore, MD, USA). The C-arm CT was acquired using *syngo* DynaCT (Siemens AG, Healthcare Sector, Forchheim, Germany) [10] and had a 3-D spatial resolution of 0.25 mm [2]. The C-arm system has a flat-panel detector with a 2-D spatial resolution of 0.308 mm. The center coordinates of the objects were extracted from the 3-D data set (*syngo* DynaCT, Siemens AG, Healthcare Sector, Forchheim, Germany) and used as ground truth to calculate the 3-D localization error. The idealized projection geometry is defined by an

SID of 120 cm, an SISOD of 75 cm and a pixel spacing of 0.308 mm. Although fixed for our experiment, the SID can be varied depending on the clinical needs at hand. In theory, a C-arm would be able to reach every position on the surface of a 3-D sphere. In practice, this is not possible, due to mechanical constraints and the table which gets in the way for certain viewing directions. For example, a position of $\beta = \pm 90^o$ would lead to a collision between the table and either the X-ray source or the detector. As a consequence, the angle α ranged from -90° to 90°, while β ranged from -45° to 45°. Both were sub-sampled in steps of 15° for simulation and experiment.

4   Results and Discussion

The results of the simulation are given in Table 1 and for the existing system in Table 2. As one would expect, the localization error is at its lowest point at an angular difference close to 90°. This does not only hold for the primary and secondary angle, but also for combinations as long as the combined angular difference is roughly about 90°. Note that, some viewing angles considered for the study are not reachable in a clinical setup, as a patient would further reduce the possible angulation with respect to a cranial/caudal position. As a simple rule of thumb, when using a C-arm system for 3-D point localization try to get a primary angular difference of around 90° first. Then attempt to increase the secondary angular difference as much as possible. Unfortunately, due to mechanical C-arm constraints this is easier said then done. Nevertheless, one should at least try to get the primary angular difference as close to 90° as possible. However, even if this is not possible, good results can still be achieved. For example, in our experiment involving a real C-arm system, we obtained an error of up to 1.18 mm if the angular difference of the primary angle was larger than 60° yet smaller than 120°. Changing the angular difference of the secondary angle was found to add improvement as long as the angular difference between the viewing directions (optical axes) was increased. Thus, considering a primary angular difference of 60°, increasing the secondary angular difference would improve the localization accuracy. Considering a primary angular difference of 120°, increasing the secondary angular difference would, however, worsen the result, as the resulting angular difference for the viewing direction increased towards 180°. In theory, a localization error of 0.81 mm is possible. Our actual C-arm system can achieve a localization accuracy that is about 1 mm. From this we conclude that 3-D point localization using a C-arm system is feasible, and it can achieve similar accuracy as electromagnetic systems [11] or optical localization systems [12]. First results in a clinical environment demonstrating this were shown in [5, 6, 13].

References

1. Prümmer, M., Wigström, L., Hornegger, J., Boese, J., Lauritsch, G., Strobel, N., Fahrig, R.: Cardiac C-arm CT: Efficient Motion Correction for 4D-FBP. In Smith,

Idealized C-Arm System: Localization Error							
		$\Delta\beta$					
		0°	15°	30°	45°	60°	75°	90°
$\Delta\alpha$	0°		2.38	1.35	1.02	0.88	0.83	0.82
	15°	2.52	1.81	1.25	1.00	0.87	0.83	
	30°	1.42	1.29	1.08	0.93	0.85	0.82	
	45°	1.07	1.03	0.94	0.87	0.82	0.81	
	60°	0.92	0.90	0.86	0.83	0.81	0.81	
	75°	0.84	0.83	0.82	0.81	0.81	0.82	
	90°	0.81	0.81	0.81	0.81	0.82		
	105°	0.82	0.82	0.82	0.84	0.86		
	120°	0.85	0.86	0.88	0.91	0.95		
	135°	0.94	0.95	0.99	1.04	1.12		
	150°	1.13	1.16	1.25	1.31			
	165°	1.66	1.65	2.13	1.86			

Table 1. The 3-D localization error in mm using projection matrices calculated from the mathematical model of an idealized C-arm system.

Real C-Arm System: 3-D Localization Error							
		$\Delta\beta$					
		0°	15°	30°	45°	60°	75°	90°
$\Delta\alpha$	0°		2.95	1.66	1.26	1.09	1.02	1.02
	15°	3.15	2.24	1.54	1.23	1.08	1.02	
	30°	1.76	1.59	1.33	1.15	1.05	1.01	
	45°	1.33	1.27	1.16	1.07	1.01	1.00	
	60°	1.13	1.11	1.06	1.02	0.99	0.99	
	75°	1.04	1.03	1.01	0.99	0.99	1.02	
	90°	1.00	0.99	0.99	1.00	1.01		
	105°	1.01	1.01	1.02	1.04	1.07		
	120°	1.06	1.06	1.09	1.13	1.18		
	135°	1.17	1.18	1.23	1.30	1.42		
	150°	1.40	1.44	1.56	1.65			
	165°	2.06	2.05	2.68	2.39			

Table 2. The 3-D localization error in mm for a real C-arm system using projection matrices obtained from a calibration run.

G.C., ed.: Nuclear Science Symposium, Medical Imaging, San Diego, CA, USA (November 2006) 2620–2628

2. Strobel, N., Meissner, O., Boese, J., Brunner, T., Heigl, B., Hoheisel, M., Lauritsch, G., Nagel, M., Pfister, M., Rührnschopf, E.P., Scholz, B., Schreiber, B., Spahn, M., Zellerhoff, M., Klingenbeck-Regn, K.: Imaging with Flat-Detector C-Arm Systems. In Reiser, M.F., Becker, C.R., Nikolaou, K., Glazer, G., eds.: Multislice CT (Medical Radiology / Diagnostic Imaging). Springer (2009 (third edition)) 33–51

3. Rougee, A., Picard, C.L., Trousset, Y.L., Ponchut, C.: Geometrical calibration for 3D x-ray imaging. In Kim, Y., ed.: Proceedings of SPIE Medical Imaging 1993: Image Capture, Formatting, and Display. Volume 1897., Newport Beach, CA, USA, SPIE (February 1993) 161–169

4. Richter, G., Pfister, M., Struffert, T., Engelhorn, T., Dölken, M., Dörfler, A.: Visualization of self-expandable stents using 2D-3D coregistration of angiographic computed tomography data to facilitate stent assisted coil embolization of broad based intracranial aneurysms: in vitro feasibility study. In: 42. Jahrestagung der Deutschen Gesellschaft für Neuroradiologie (DGNR 2007). (2007)

5. Meyer, B.C., Brost, A.B., Yatziv, L., Strobel, N., Gilson, W., Wolf, K.J., Lewin, J.S., Wacker, F.K.: Image-Guided Percutaneous Punctures Using a Combined MR Imaging / C-Arm CT Approach: A Pilot Study assessing the Feasibility. In: Proceedings of ISMRM 2008 - 16th Scientific Meeting and Exhibition, International Society for Magnetic Resonance in Medicine (May 2008)

6. Meyer, B.C., Brost, A.B., Yatziv, L., Strobel, N., Gilson, W., Kraitchman, D., Lewin, J.S., Wacker, F.K.: Punctures in a hybrid MR/X-ray Angiographysuite using MR image overlay and stereoscopic x-ray navigation: A study in Phantoms, Animals and a Patient. In: Proceedings of ISMRM 2009 - 17th Scientific Meeting and Exhibition, International Society for Magnetic Resonance in Medicine (April 2009)

7. Fajardo, L., Willison, K., Pizzutiello, R.: A comprehensive approach to stereotactic breast biopsy. Blackwell Science Inc, Boston, MA (1996)

8. Brost, A., Strobel, N., Yatziv, L., Gilson, W., Meyer, B., Hornegger, J., Lewin, J., Wacker, F.: Accuracy of x-ray image-based 3D localization from two C-arm views: a comparison between an ideal system and a real device. In Miga, M.I., Wong, K.H., eds.: Medical Imaging 2009: Visualization, Image-Guided Procedures, and Modeling. Volume 7261., Lake Buena Vista, FL, USA, SPIE (2009) 72611Z

9. Fahrig, R., Holdsworth, D.W.: Three-dimensional computed tomographic reconstruction using a C-arm mounted XRII: Image-based correction of gantry motion nonidealities. Medical Physics **27**(1) (January 2000) 30–38

10. Zellerhoff, M., Scholz, B., Ruehrnschopf, E.P., Brunner, T.: Low contrast 3D reconstruction from C-arm data. In Flynn, M.J., ed.: Proc. of SPIE Medical Imaging 2005: Physics of Medical Imaging. Volume 5745., SPIE (2005) 646–655

11. Nagel, M., Hoheisel, M., Petzold, R., Kalender, W.A., Krause, U.H.W.: Needle and catheter navigation using electromagnetic tracking for computer-assisted C-arm CT interventions. In Cleary, K.R., Miga, M.I., eds.: Proceedings of SPIE Medical Imaging 2007: Visualization and Image-Guided Procedures. Volume 6509 of Proc. of SPIE. (2007) 65090J–1–65090J–9

12. West, J.B., Maurer, C.R.: Designing Optically Tracked Instruments for Image-Guided Surgery. IEEE Transactions on Medical Imaging **23**(5) (2004) 533–545

13. Meyer, B.C., Brost, A., Strobel, N., Wacker, F.K.: Abstract No. 110: Fluoroscopy Guided Punctures in a Flat Detector C-Arm System: Evaluation of Stereoscopic Needle Tracking Based on Cone Beam CT Images. Journal of Vascular and Interventional Radiology **20**(2) (February 2009) 43–44